

**Cavity-Containing Aromatic Oligoamide Foldamers and
Macrocycles: Progress and Future Perspectives**

| | |
|-------------------------------|--|
| Journal: | <i>Organic & Biomolecular Chemistry</i> |
| Manuscript ID | OB-REV-08-2022-001467 |
| Article Type: | Review Article |
| Date Submitted by the Author: | 12-Aug-2022 |
| Complete List of Authors: | Sobiech, Thomas; University at Buffalo, Department of Chemistry Zhong, Yulong; University at Buffalo, Department of Chemistry Gong, Bing; University at Buffalo, Department of Chemistry |
| | |

ARTICLE

Cavity-Containing Aromatic Oligoamide Foldamers and Macrocycles: Progress and Future Perspectives†

Thomas A. Sobiech,^a Yulong Zhong^a and Bing Gong^{*a}

Received 00th January 20xx,
Accepted 00th January 20xx

DOI: 10.1039/x0xx00000x

As a major class of foldamers, aromatic oligoamide foldamers have attracted intense interest. The rigidity of aromatic residues and amide linkages allows the development of foldamers with readily predictable, stable conformations. Aromatic oligoamide foldamers having backbones fully constrained by intramolecular hydrogen bonds have attracted wide attention. Depending on their lengths, such foldamers adopt crescent or helical conformations with highly negative inner cavities. Cyclizing the backbone of the aromatic oligoamides afford the corresponding macrocycles which are featured by persistent shapes and non-deformable inner cavities. With their defined, inner cavities, such aromatic oligoamide foldamers and macrocycles have served as hosts for cationic and polar guests, and as transmembrane channels for transporting ions and molecules. Recent synthetic progress resulted in the construction of multi-turn hollow helices that offer three-dimensional inner pores with adjustable depth. Reducing the number of backbone-constraining hydrogen bonds leads to oligoamides which, with their partially constrained backbones, undergo either solvent- or guest-dependent folding. One class of such aromatic oligoamide foldamers, which offer multiple backbone amide NH groups as hydrogen-bond donors, are designed to bind anions with adjustable affinities.

1. Introduction

Protein folding involves a multitude of non-covalent interactions that work synergistically to yield complex structures with innumerable functionality.¹ Although elaborate, proteins are composed of comparatively simple building blocks. This realization prompted chemists to explore alternative building blocks for the creation of new folded structures. Since

Gellman and Seebach published their work on β -peptides in the mid-1990s,² many foldamers have become known.³

A diverse range of approaches has been adopted for the development of foldamers by taking advantage of non-covalent interactions such as hydrogen bonding, ionic, aromatic stacking, ion-dipole, solvophobic, and halogen bonding interactions. Foldamers can be roughly grouped into those having peptidomimetic^{2,4} and abiotic⁵ backbones.

Aromatic oligoamide foldamers, which can be regarded as being both peptidomimetic and abiotic, are a unique class of foldamers featuring rigid backbones and well-defined, stably folded conformations.⁶ The seminal work of Hamilton demonstrated that aromatic oligoamides with intramolecular

^a Department of Chemistry, University at Buffalo, the State University of New York, Buffalo, NY 14260, USA

† This work is dedicated to Professor David G. Lynn in celebration of his 70th birthday



Thomas A. Sobiech

Thomas Sobiech graduated from the State University of New York at Oswego in 2017 with a Bachelor of Science in biochemistry. He is currently a PhD candidate at the University at Buffalo under the direction of Professor Bing Gong. His research has focused on the synthesis and characterization of aromatic oligoamide foldamers and macrocycles, with an emphasis on developing host-guest systems with high binding affinity and strong positive cooperativity.



Yulong Zhong

Yulong Zhong received his PhD degree in organic chemistry from Beijing Normal University, Beijing, China, in 2016. He then joined Professor Bing Gong's group at the State University of New York at Buffalo as a postdoctoral associate. As a research scientist, he is currently focusing on the synthesis and study of multiturn helical aromatic oligoamides as novel hosts for guest binding and as transmembrane channels for ion and molecular transport.

hydrogen bonds being introduced between adjacent residues could adopt folded conformations in the solid state.⁷

Our group proposed and created cavity-containing or hollow aromatic oligoamide foldamers with backbones fully constrained by intramolecular three-center hydrogen bonds with extraordinary stability.⁸ The basic units of our foldamers are exemplified by amides **1** and **2** which adopt nearly planar crescent conformations enforced by the three-center hydrogen bond(s) composed of S(5)- and S(6)-type⁹ intramolecularly hydrogen-bonded rings. Aromatic oligoamides with partially constrained backbones are also possible through the incorporation of two-center intramolecular hydrogen-bonds along the backbone,¹⁰ with the basic units of such oligoamides being illustrated by amides **3** and **4**. Additional hydrogen bonded scaffolds have been developed with the intramolecular interactions occurring on the interior of the oligomer (amides **5-8**). These eight scaffolds enable a diverse range of aromatic oligoamides to fold by following the same principle, i.e., backbone-constraining with highly favorable, localized intramolecular hydrogen bonds (Fig. 1).

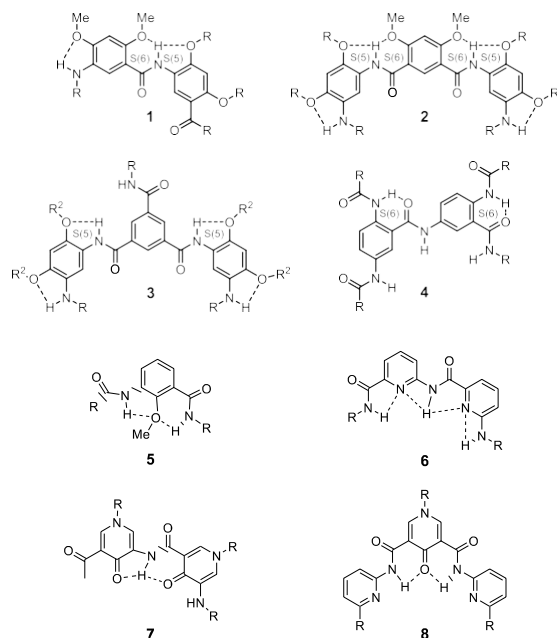


Fig. 1 Various hydrogen bonding scaffolds discussed in this review.

An incredible amount of variety is possible through the incorporation of these eight basic backbones in the development of foldamers and macrocycles. These building blocks enable the fine tuning of cavity size, length, and electronics. Preorganization and rigidification lead to the highly efficient synthesis of macrocycles with fundamentally new properties as hosts for various guest molecules as well as self-assembled superstructures. These non-covalently programmed structures are continuously being developed and refined and here we present some of the most recent (and historical) advancements in their construction and application.

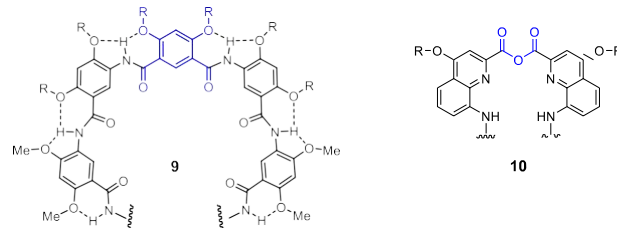


Fig. 2 General structures of oligoamides a symmetrical backbone consisting of a central diacid **9** or anhydride **10** residue (blue) and two identical groups. Reprinted with permission from ref. 16 and 23. Copyright 2020 American Chemical Society.

2. Crescent and Helical Foldamers with Constrained Aromatic Oligoamide Backbones

2.1. The Creation of Multiturn Helices

In 2000, we reported folding oligomers consisting of 5-amino-2,4-dialkoxybenzoic acid residues as shown by general structure **1**.¹⁴ The aromatic amide backbone of such an oligomer is constrained by highly stable intramolecular hydrogen bonds. The rigidity of the amide linkages and the *meta*-linked aromatic rings, along with the restricted rotation of the aryl-amide single bonds, imparts curvature to the aromatic backbone, leading to folded conformations containing electrostatically negative cavities with multiple convergently placed carbonyl oxygens. Oligoamides with an unsymmetrical backbone having a *N*-to-*C* direction and up to eight residues could be synthesized via stepwise amide coupling. Symmetrical oligoamides **9** with up to nine residues were also synthesized through a convergent route by coupling two amino-terminated short oligomer precursors with a central diacid unit (Fig. 2).¹⁵ A similar approach was taken by Huc who synthesized impressively long oligomers with quinoline-based aromatic oligoamide backbones through segment doubling using an anhydride linker (Fig. 2, anhydride **10**).¹⁶ This strategy enabled the synthesis of a 96mer via condensation of two 42mer amino fragments. The crystal structure of a representative 48mer anhydride is seen below (Fig. 3)

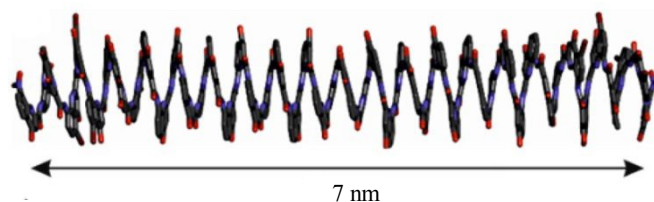


Fig. 3 Crystal structure of a 48-residue anhydride (FW = 11.7 kDa) prepared by Huc. Ref 16.

Within our system, attempts to synthesize longer oligoamides were met with increasingly poor yields as chain length extended, hypothesized to be due to steric hindrance arising from the stably folded conformations which shield reactive sites. We attempted to avoid steric hindrance via replacing each backbone amide hydrogen with a 2,4-dimethoxybenzyl (DMB) group, the folding of these oligomers was temporarily disrupted, enabling the synthesis of

symmetrical oligoamides with up to fifteen residues.¹⁷ Removing the DMB-groups under acidic conditions restored the three-center hydrogen bond, which reestablished the folded structure.

Research done by the Huc group implemented solid phase synthesis (SPS) in an attempt to streamline the synthetic process for aromatic oligoamides (specifically, quinoline oligoamides).¹⁸ SPS enables high throughput screening of foldamers composed of a variety of different building blocks for molecular recognition, materials, and biological relevance, analogous to traditional SPS for natural peptides. Their SPS procedure found low-loading Wang resin (to avoid steric hindrance of neighboring folded oligomers) and the activation of acids via the in-situ generation of acid chloride and microwave irradiation (due to the poor nucleophilicity of the aromatic amine) to be crucial for efficient coupling. This methodology was found to be highly effective in the synthesis of hybrid oligomers consisting of quinoline oligoamides and natural α -amino acids, paving the way for new biologically relevant applications.¹⁹

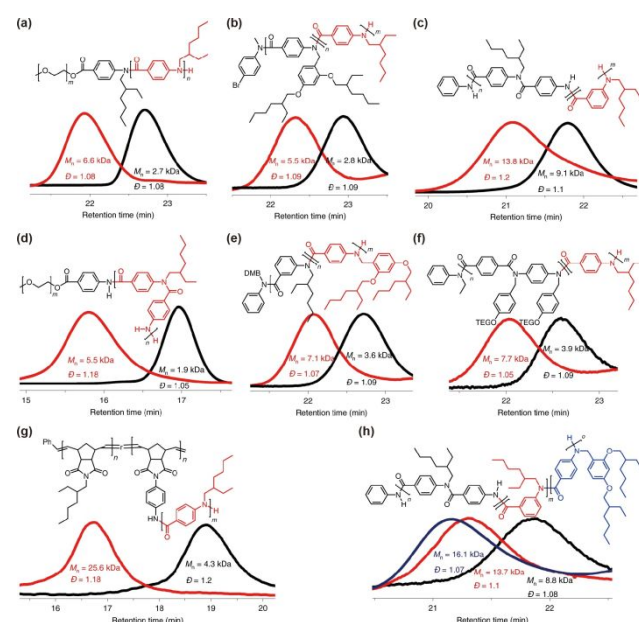


Fig. 4 GPC analysis of copolymers prepared by Kilbinger. Ref 21

Efforts to synthesize continuous multiturn aromatic oligoamides with discrete lengths still proved to be challenging which led researchers to explore polymerization strategies to achieve this goal. In attempts to synthesize oligomers with lengths that could match the thickness of lipid bilayers (25 to 40 Å) we reported the synthesis of polyamides in 2012.²⁰ These polyamides consisted of partially rigidified backbones with general structure **3**. Polyamides of up to roughly 18 turns were determined by GPC with narrow length distributions. Kilbinger and coworkers were successful in the synthesis of a variety of polyamides through controlled, living polymerization.²¹ This versatile method afforded a plethora of polyamides (including diblock copolymers and triblock tripolymers) with impressively narrow dispersity (Fig. 4).

Recent screening by Zeng has found the most efficient amide coupling reagents for the synthesis of multiturn cavity containing aromatic polyamides composed of alternating pyridine-pyridone building blocks, amide **11** (Fig. 5).²² They found that the coupling reagent PyBOP lead to the efficient formation of polyamides capable of spanning the lipid bilayer with channel lengths of 3.4 nm. These channels due to their tight inward pointing intramolecular hydrogen bonding possess narrow cavity diameters of 3 Å. Interestingly, these cavities were found to be excellent artificial proton transporters with rates 1.2 and 11 times faster than gramicidin A and M2 channels, respectively. This transport also took place with exceptional selectivity for protons over Cl⁻, Na⁺ and K⁺ ions.

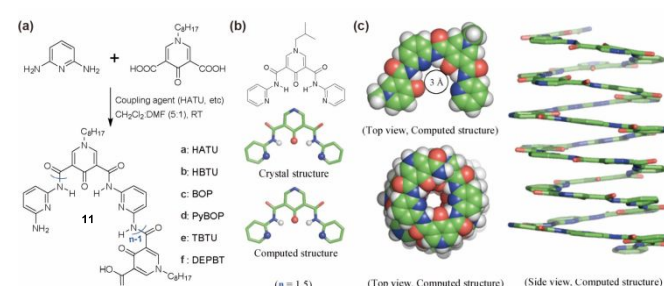


Fig. 5 Hybrid pyridine-pyridone polyamides. a) One-pot synthesis of polyamides using a variety of different coupling reagents. b) Inward facing hydrogen-bonded backbone c) Computed structures for multiturn helices. Ref 22.

We have made major recent progress in synthesizing longer oligoamides of defined lengths. In 2020, we reported the synthesis of oligoamides that fold into multi-turn helices (Fig. 6).²³ The longest oligomer obtained was 24mer **12i**. The crystal structure of 16mer **12g** was determined, revealing a compact helix of over 2.5 turns. Optimization of protecting groups, coupling conditions and purification methods enabled the synthesis of these longer oligomers.

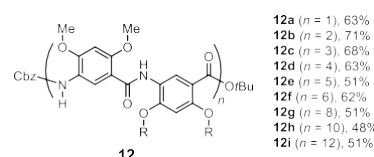


Fig. 6 Series of continuous backbone aromatic oligoamides synthesized ranging from dimer (**12a**) to 24mer (**12i**).

The synthesis of this series of oligoamides involved removing the *N*-terminal Cbz group or the *C*-terminal *t*-butyl group of dimer **12a**, affording the corresponding dimer amine and dimer acid which were coupled by treating with HBTU in the presence of *N,N*-diisopropylethylamine (DIEA) in CH₂Cl₂ to give tetramer **12b**. Repeating these cycles of deprotection and coupling afforded longer oligomers **12c** – **12i** in good yields. The coupling steps proceeded with similar efficiency regardless of the fragment being coupled, i.e., the coupling of dimer, tetramer or octamer amines to the growing oligomer acid gave similar yields.

Detailed structural studies using 2D NMR enabled the unambiguous assignment of each individual residue for

oligoamides **12d** – **12i**.²³ In the mixed solvent DMSO-*d*₆/CDCl₃, numerous NOE contacts were observed between amide or aromatic protons of residues 6-7 units apart, confirming that these helices are remarkably stable and compact even in a polar solvent (Fig. 7).

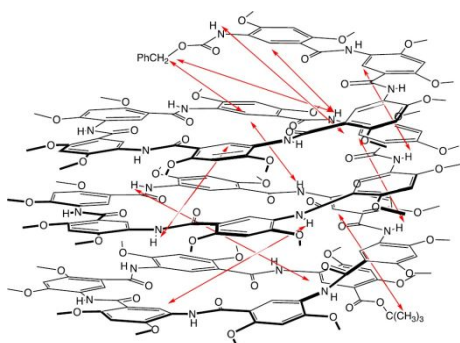


Fig. 7 Conformation of 20mer **12h** drawn based on energy-minimized helical structure, supported by NOEs (red arrows) revealed by the NOESY spectrum of **12h**. Reprinted with permission from ref. 23. Copyright 2020 American Chemical Society.

Single crystals of 16mer **12g** were obtained via slow liquid-liquid diffusion, which led to the determination of the first crystal structure of a multiturn helical oligoamide of this series (Fig. 8).²³ The structure of **12g** reveals a compact helix having 6.6 residues per turn, a helical pitch of 3.4 Å and an inner cavity of ~9 Å across. A sodium ion solvated by water and methanol molecules resides at the center of the helix, suggesting the inner pores of our helical oligoamides are amenable to accommodating cations and polar molecules. In work yet to be published we have found that the electronegative pockets of these folding oligoamides exhibit extraordinary binding affinities for bipyridinium-based cationic guests.

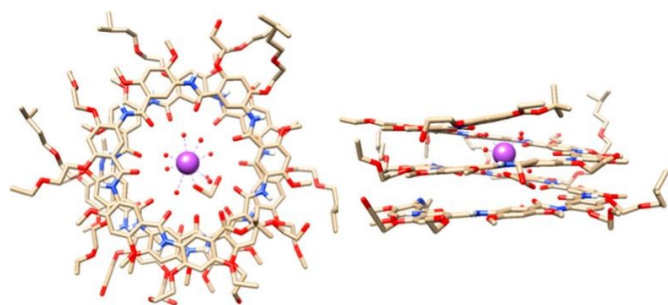


Fig. 8 Top and side views of the crystal structure of 16mer **7g**. Reprinted with permission from ref. 23. Copyright 2020 American Chemical Society.

Oligoamides **12g** – **12h** have cylindrical inner cavities. However interesting work by Huc has been geared towards the synthesis of nonuniform folded capsules²⁴ offering unique features for molecular recognition such as complete encapsulation, exclusion of solvent as well as slow dissociation kinetics, making these folding oligoamides viable candidates in sensors and drug delivery. These capsules are constructed from a variety of unique monomer building blocks with differing lengths and non-covalent interactions. The assembly of this monomer library enables the fine tuning of helical diameter within the folded structure. The rational design of helical

capsules with sequence dependent intermolecular interactions as well as defined cavity volumes were found to recognize chiral organic acids and monosaccharides with modest binding affinity as well as selectivity.

Huc demonstrated the power of his structure-based iterative evolution approach for foldamer sequences through the successful synthesis of a fructose specific molecular capsule.²⁵ A monomer library (Fig. 9) is used in the construction of a first-generation receptor which is screened and further modified to enhance size-shape complementarity as well as favorable sequence dependent hydrogen bonding interactions. Viable foldamer sequences were improved through additions, mutations, and deletions to yield a highly selective fructose receptor. These efforts afforded a capsule with binding affinity 300 times better for fructose than mannose, which is highly challenging. This process incorporated a variety of methods including computational modeling, detailed crystal structure analysis as well as one- and two-dimensional solution state NMR studies.

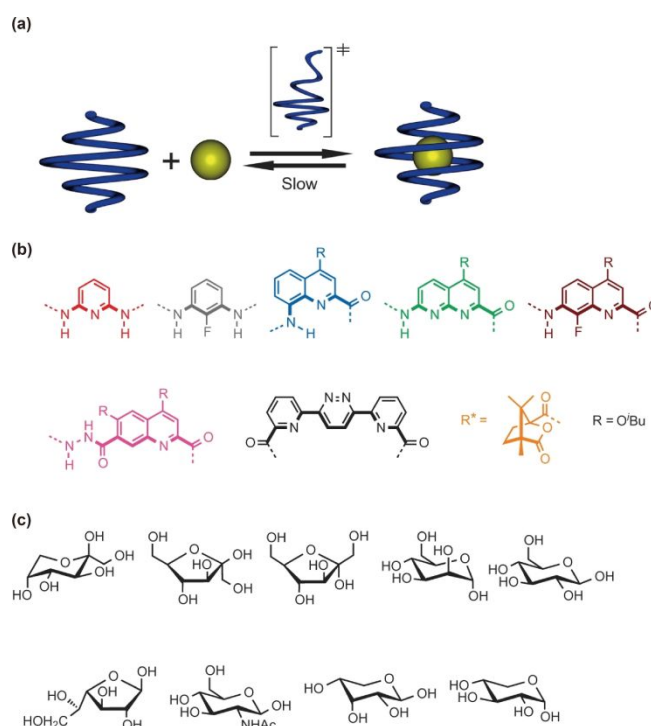


Fig. 9 Host-Guest components used in the construction of a selective fructose capsule.

(a) Kinetics detailing slow guest capsule encapsulation. (b) Monomer library. (c) Monosaccharide guests. Ref 25.

2.2. Self-Association of Short Aromatic Oligoamides

Inter-turn aromatic stacking interactions play an important role in stabilizing multi-turn helices, resulting in compact helical conformations. With relatively large and flat aromatic and amide surfaces, these oligoamides may also engage in strong intermolecular interactions enabling the formation of higher order aggregates. We investigated the role oligomer length, solvent and temperature played in the intermolecular

interactions of a series of short crescent aromatic oligoamides (Fig. 10).²⁶

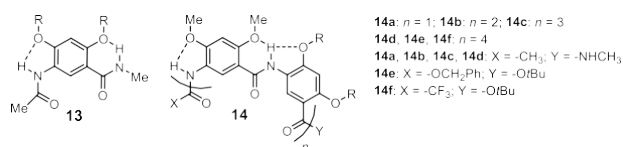


Fig. 10 Short continuous backbone aromatic oligoamides used for detailed aggregation study. Reprinted with permission from ref. 26. Copyright 2018 American Chemical Society.

The 1H NMR spectra of oligoamides **13** – **14** in $CDCl_3$ showed that amides **13** and **14a** displayed sharp signals, tetraamide **14b** exhibited slightly broadened signals with the longer **14c** and **14d** giving the most severely broadened signals. The broadening of 1H NMR signal was presumably due to restricted molecular motion of oligoamide molecules constituting the aggregates. The correlation of aggregation with oligomer length was probed by using fluorescence spectroscopy. A non-linear increase in emission intensity at 438 nm was observed with increasing oligomer length, with dimer **14a** showing no fluorescence emission (Fig 11a). The emission bands were found to be broad and featureless, indicative of excimer-like emission typical of π -stacked aggregates. With increasing length, these crescently-shaped oligoamides provide increasing overall surface area, resulting in enhanced self-association. For oligoamides bearing six or more residues, strong stacking interactions become apparent.

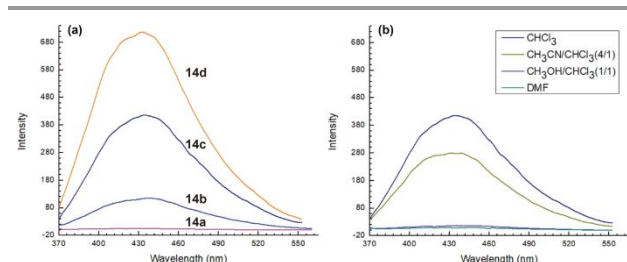


Fig. 11 Emission spectra of (a) oligoamides **9a-9d** ($10 \mu M$) in $CHCl_3$ and (b) hexamer **9c** ($10 \mu M$) in various solvents. Reprinted with permission from ref. 26. Copyright 2018 American Chemical Society.

The sharpening of NMR signals along with fluorescence quenching was observed upon the addition of polar solvents such as DMSO, DMF, MeOH, and MeCN. The polarity as well as the hydrogen-bonding capability of the solvent appears to be the dominant factor in dissipating the aggregation. The ability of a solvent to dissociate the aggregates was initially believed to be correlated with its dielectric constant. However, we found that the hydrogen-bond donating potential of a solvent may be a more accurate predictor for its ability to disrupt aggregation. For instance, the emission intensities of oligoamides **14c** and **14d** are much lower in the less polar solvent system $CH_3OH/CHCl_3$ (1/1, v/v , $\epsilon = 19$) than in $CH_3CN/CHCl_3$ (4/1, v/v , $\epsilon = 31$) (Fig. 11b). Solvents with larger dielectric constants can engage in dipole-dipole interactions most likely with the polar aromatic amide backbones, whereas solvents with good hydrogen-bond donating capabilities can participate in multiple

hydrogen bonds with the acceptor oxygen atoms of the amide groups and the ether sidechains of the oligoamides.

Variable-temperature fluorescence studies demonstrated that the aggregation/deaggregation process may proceed cooperatively. As the temperature was increased the emission intensity was found to decrease significantly. In solvents such as $MeCN/CHCl_3$ (4/1) in which the aggregation was significantly weakened, a sigmoidal curve was obtained by plotting the emission intensity versus temperature. This observation indicated that the self-assembly of these oligomers proceeds cooperatively, with an abrupt transition from an aggregated to an unaggregated state.

Previously mentioned aromatic oligoamides aggregate through aromatic stacking interactions promoted in non-polar solvents, which may result in extended columnar assemblies. In an effort to guide directional assembly Li and coworkers modified general structure **2** with halogen containing functional groups for intermolecular halogen bonding interactions.²⁷ In the solid state these short oligoamide fragments were found to form helical arrangements which further associated to form double and even quadrupole helices. This clever approach could facilitate the development of new self-assembled cavity containing aromatic oligoamides.

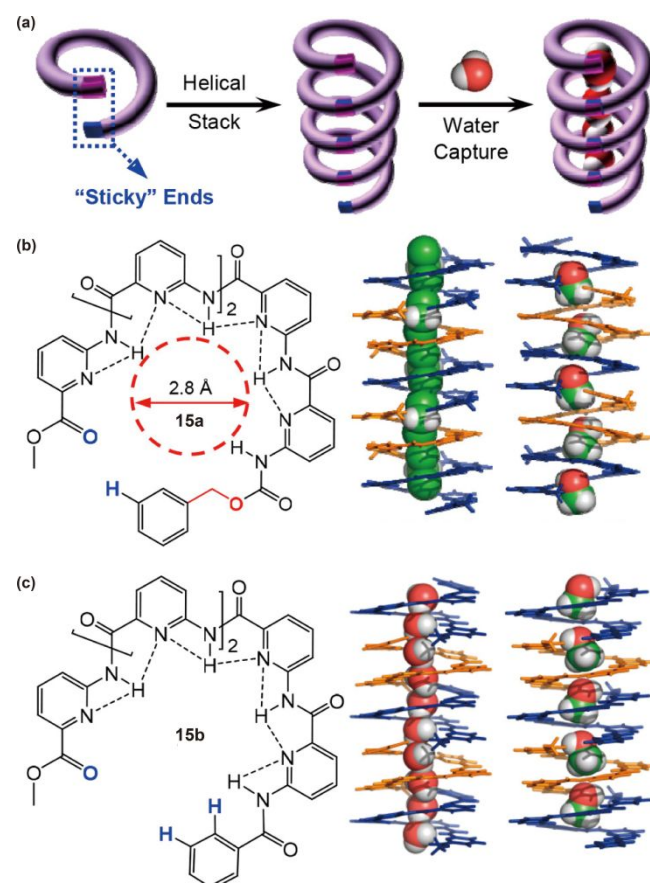


Fig. 12 Molecular design and representative crystal structures of aquafoldamer-based artificial water channels developed by Zeng. (a) "Stick end" approach for the self-assembly of 1D nanotubes using short oligomers. (b) and (c) Chemical and crystal structures of monomers and self-assembled channels with various solvent molecules encapsulated. Ref 28

Short disk-like aromatic oligoamides (**15a** and **15b**) which contain inward pointing three-center hydrogen bonding interactions were designed with "sticky ends" for favorable directional assembly by Zeng and coworkers (Fig. 12).²⁸ These helical assemblies with their narrow inner cavities (2.8 Å) with favorable hydrogen bonding interactions were found to act as highly efficient synthetic water channels. These "aquafoldamers" rivaled natural aquaporins with high water transport of $\sim 3 \times 10^9 \text{ H}_2\text{O S}^{-1} \text{ channel}^{-1}$. These channels also exhibited high selectivity for water with rejection of NaCl and KCl salts.

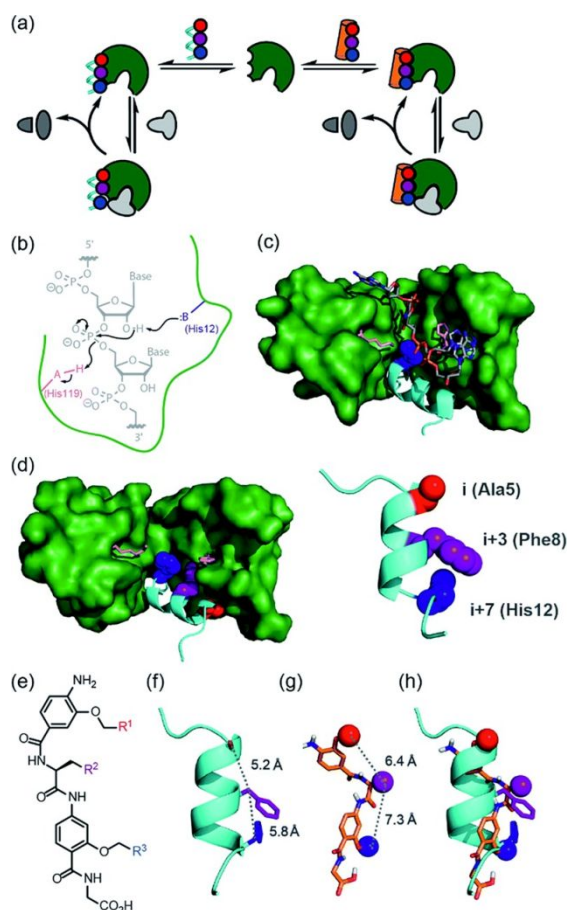


Fig. 13 Wilson's general approach for the construction of a functional protein-proteomimetic complex. (a) Replacement strategy of a non-covalent peptide protein segment with a proteomimetic sequence. (b) General acid-base catalysis of RNA hydrolysis. (c) X-Ray crystal structure of bovine ribonuclease A (green). (d) X-ray crystal structure of bovine ribonuclease S-protein (green)/S-peptide (cyan) complex highlighting key catalytic residues. (e) chemical structure of an oligoamide foldamer designed to mimic α -helices. (f) S-peptide α -helix illustrating the side-chains. (g) molecular model of the oligoamide foldamer. (h) overlay of the α -helix and the foldamer. Ref 30

2.3. Biological Application of Aromatic Oligoamide Foldamers

The incorporation of aromatic oligoamide foldamers in biological applications has been a major focus in recent years. Short aromatic oligoamides have been developed by Wilson to mimic α -helices (Fig 13e). These short sequences are structurally defined and have tunable sidechains.²⁹ Wilson demonstrated that these short oligomers could interact with large protein structures and can even restore catalytic function

to an RNase (responsible for RNA degradation) (Fig. 13).³⁰ They studied this by removing a catalytically active small peptide known as the S-peptide from RNase S. The S-peptide interacts with the RNase protein via a small cleft and contains one of the active histidine residues responsible for acid-base hydrolysis of the phosphodiester linkage in RNA. Their small oligoamide mimics the S-peptide with an active imidazole sidechain and was found to restore catalytic activity in the S-peptide deficient RNase. These findings demonstrate that significant portions of proteins could be replaced by abiotic foldamers, opening the door to new research in foldamer based therapeutics and sensors.

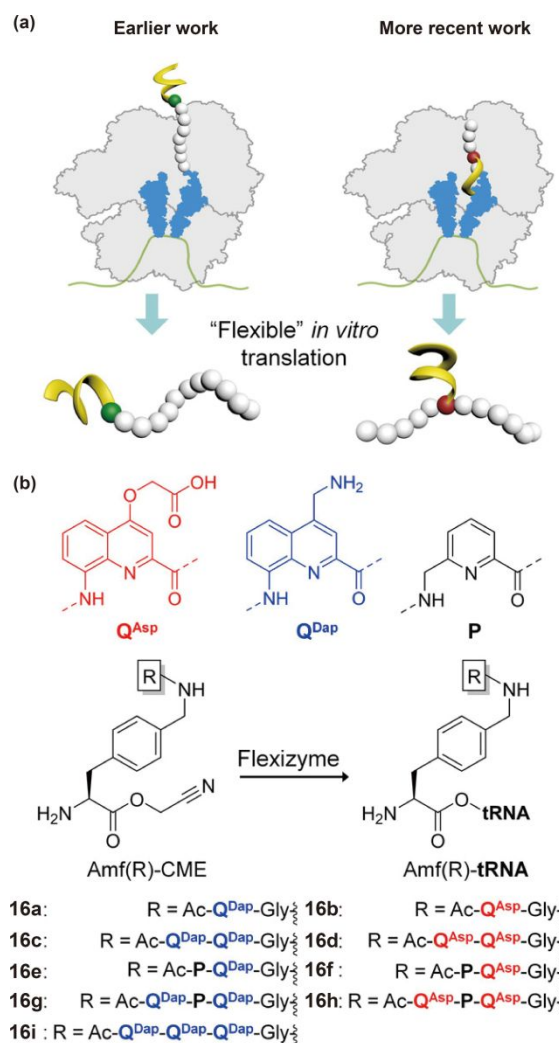


Fig. 14 (a) Cartoon depiction of the translation of amino-acid residues modified with aromatic oligoamide foldamers by the ribosome both at the N-terminus (left) and within the growing peptide sequence (right). (b) Aromatic oligoamide monomers attached to a modified phenylalanine residue which is further incorporated onto tRNA via flexizyme activity. Ref 33.

Other research has focused on the possibility for biological systems to accept and even incorporate abiotic residues into their natural sequences. Research by Suga found that non-

natural amino acids could be incorporated into tRNAs via flexizymes, which enables them to be processed via the ribosome.³¹ Huc and Suga together reported the incorporation of aromatic oligoamides consisting of quinoline and pyridine residues into peptide sequences using this approach (Fig. 14).³² Initially, it was found that these foldamer-peptide hybrids could only incorporate unnatural residues as the final residue during translation.³³ However, recently they demonstrated the ability to incorporate these unnatural monomers into the center of the growing peptide.

that the ribosome is far more tolerant to alternative building blocks than previously thought. Future work in this area could see additional foldamer peptide hybrid oligomers or even complete abiotic sequences synthesized by the ribosome via flexizyme activity.

3. Aromatic Oligoamide Macrocycles

3.1. Macrocycles with Backbones Fully Constrained by Peripherally Placed Hydrogen Bonds

In 2004, our group reported the one-pot formation of aromatic oligoamide macrocycles **17** consisting of alternating diacid and diamine residues.³⁴ This class of macrocycles contains a backbone fully constrained by intramolecular three-center hydrogen bonds. The interior of the macrocyclic backbone carries rigidly held carbonyl oxygen atoms, resulting in an electronegative cavity. These disc-like molecules were found to bind cationic guests, undergo self-aggregation to form tubular assemblies capable of transporting ions and small molecules across a bilayer.

¹H NMR studies revealed broad, featureless signals in nonpolar solvents such as chloroform, confirming the strong aggregation of these macrocycles. The stacking interactions of the macrocycles could be disrupted by adding polar solvents such as DMSO, DMF, MeOH or MeCN. Large downfield shifts and sharpening of resonances are observed for aromatic and amide protons during titration experiments with polar solvent.³⁵ These aggregates were speculated to undergo anisotropic aggregation, leading to tubular assemblies.

With six convergently placed amide carbonyl oxygen atoms, the cavity of these macrocycles is highly electronegative and thus strongly complexes cationic guests. Initial findings demonstrated that the cavity of these macrocycles could interact weakly with tetraethyl ammonium cations via ion dipole interactions.³⁶ A simple computational modeling suggested that the guanidinium ion would fit nearly perfectly within the cavity of **17** (Fig. 16).³⁷ Macrocycle **17** was found to bind to the guanidinium ion selectively even in the presence of a variety of other cations. Two-dimensional NMR spectra also revealed strong NOEs between the internal aromatic protons and the NH₂ protons of guanidinium, confirming the binding of the guanidinium inside the cavity of the macrocycle.

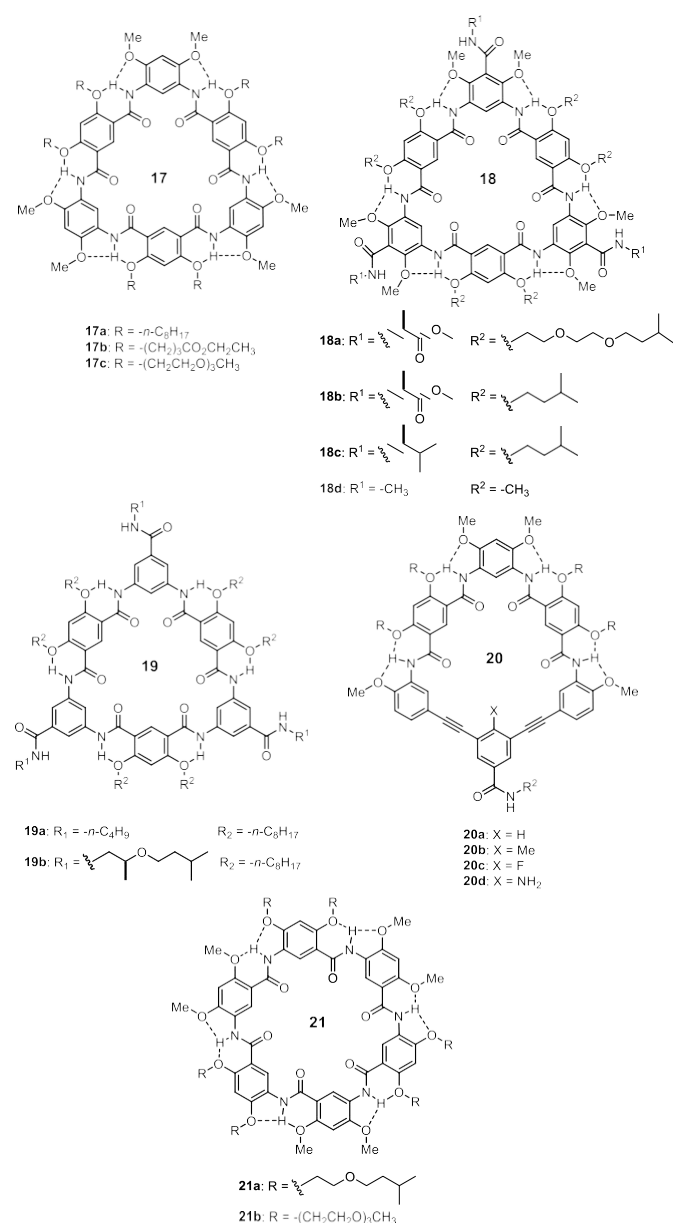


Fig. 15 General structures of aromatic oligoamide macrocycles discussed in this work.

These unnatural monomers were first incorporated onto the sidechain of a 4-(aminomethyl)-L- α -phenylalanine residue (Amf) which is capable of being recognized by the flexizyme. It was previously thought that the bulky Q building block would impose too much steric strain onto the peptide due to the rigidity of the quinoline core however their results demonstrate



Fig. 16 Computational modeling of macrocycle **10** with the guanidinium cation in the cavity. Reproduced from ref. 37 with permission from the Royal Society of Chemistry.

Upon mixing macrocycle **17** with bipyridinium cations, a color change from clear to light yellow was observed, indicative of complex formation.³⁸ UV-Vis and ¹H NMR titrations confirmed the presence of a 2:1 complex consisting of two macrocyclic molecules and one cationic guest. Association constants were determined by nonlinear fitting of the titration curves and were found to be $K_1 = 3.49 \times 10^7 \text{ M}^{-1}$ and $K_2 = 1.09 \times 10^6 \text{ M}^{-1}$ with $K_{\text{total}} = 3.80 \times 10^{13} \text{ M}^{-2}$ in acetone, revealing exceptionally strong binding affinity.

Also, 2D NOESY experiments detailed the threading of the bipyridinium ion within the three-dimensional cavity produced by the two stacking macrocycles. X-ray crystallography provided atomic details including intermolecular stacking distances of 3.71 Å that indicate stacking interactions between the macrocycle backbones (Fig. 17, left). These pseudo[3]rotaxanes were found to template the highly efficient formation of their corresponding rotaxanes in 85% yields (Fig. 17, right). The high binding affinity of these macrocycles paves the way for more efficient modes of forming mechanically interlocked molecules.

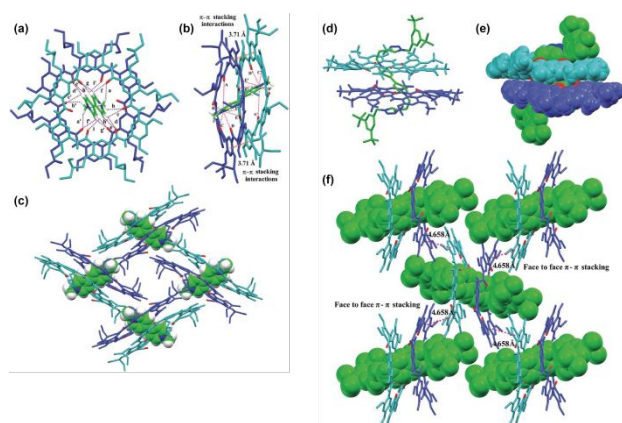


Fig. 17 X-ray crystal structure of the pseudo[3]rotaxane formed by **10** and the bipyridinium ion shown from (a) top, (b) side views, and (c) Crystal packing of the complex. X-ray crystal structure of capped rotaxane formed by **10** and the bipyridinium ion is shown in (d) capped stick model, (e) space-filling model and (f) Crystal packing structure. Reproduced from ref. 38 with permission from the Royal Society of Chemistry.

Introducing macrocycle **17** to a planar lipid bilayer, transmembrane transport of sodium and potassium ions across the membrane was observed.³⁹ Transmembrane conductance measurements indicated that macrocycle **17** exhibited much greater conductance than many natural or synthetic ion channels with the pore formed being more closely related to pore-forming toxins like α -hemolysin. The self-association of these macrocycles allows for the formation of columnar assemblies with electrostatically negative pores capable of facilitating the transport of cations across lipid bilayer (Fig. 18).

Expanded macrocycles consisting of eight residues were synthesized and studied by Yuan.⁴⁰ These macrocycles deviated from planarity with their saddle-like conformations which afforded an 11.6-Å cavity diameters. A systematic study of the binding of this new series of macrocycles with bipyridinium derivatives (varying positions of charged nitrogen) revealed strong positive cooperativity. UV-Vis titrations found that these macrocycles bind bipyridinium guests in a 2:1 ratio with

cooperativity values up to 165 with modest overall binding affinity in $\text{CHCl}_3/\text{CH}_3\text{CN}$ mixed solvent.

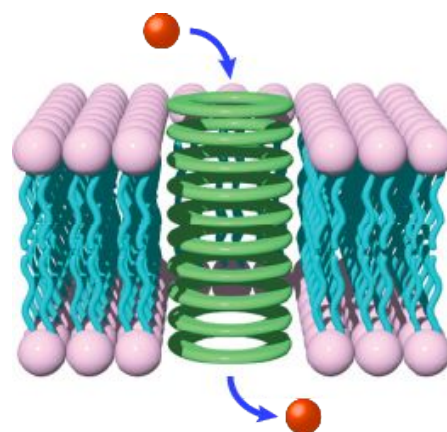


Fig. 18 Cartoon representation of the self-assembled columnar stacks of macrocycle **17** within the lipid bilayer facilitating ion transport. Reprinted with permission from ref. 39. Copyright 2008 American Chemical Society.

3.2. Macrocycles with a Backbone Fully Constrained by Internally Placed Hydrogen Bonds

Research by Zeng has provided a variety of new aromatic oligoamide macrocycles with fully constrained backbones through the implementation of an inward facing hydrogen bonding network. Initial work led to the stepwise synthesis of a linear pentamer based on a 3-amino-2-methoxybenzoic acid basic residue (Fig. 19).⁴¹ Like previously mentioned macrocycles, this series is also preorganized for intramolecular cyclization. The pentamer macrocycle was obtained in 62% yield from its linear pentamer counterpart. Using this inward pointing hydrogen bonded scaffold, the inner cavity of the macrocycle could be tuned. Incorporation of phenol -OH as well as alternative R groups to the alkoxy moiety allows for a change in cavity size, steric crowdedness, and hydrophobicity. Optimization of coupling conditions affords a method for the one-pot synthesis of this series of pentamer macrocycles with yields up to 50%.⁴² The general applicability of POCl_3 as an effective coupling reagent for this one-pot macrocyclization was seen in the synthesis of a variety of alternative pentamer macrocycles with varying alkoxy substituents within the inner cavities.

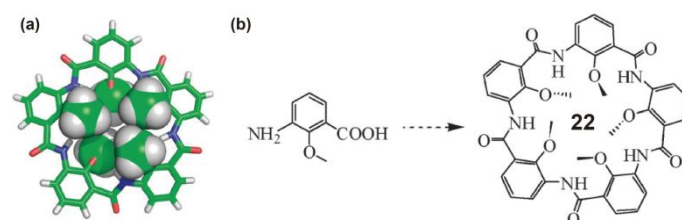


Fig. 19 a) Top view of crystal structure of **22**. b) General scheme for the one-pot synthesis of **22**. Ref 41

Zeng also provided a series of pyridone hexamer macrocycles first through cyclization of linear hexamer precursors⁴³ and eventually optimizing one-pot macrocyclization conditions under mild conditions using BOP and DIEA (Fig. 20).⁴⁴ These macrocycles possess narrow (2.9 Å) hydrophilic inner cavities and were found to

be highly efficient in the extraction of various alkali metals from aqueous into organic media with association constants calculated as high as $2 \times 10^8 \text{ M}^{-1}$ in CHCl_3 for Li^+ .⁴³ Interestingly, these macrocycles were found to have highly selective and efficient extraction capabilities for Cu^{2+} ions in artificial seawater (extraction efficiencies up to 93%).⁴⁵ Upon the addition of additional ions other than copper the extraction efficiency of the hexamer macrocycle was improved to 97% at very low $[\text{Host}]/[\text{CuCl}_2]$ ratios of 2:1.

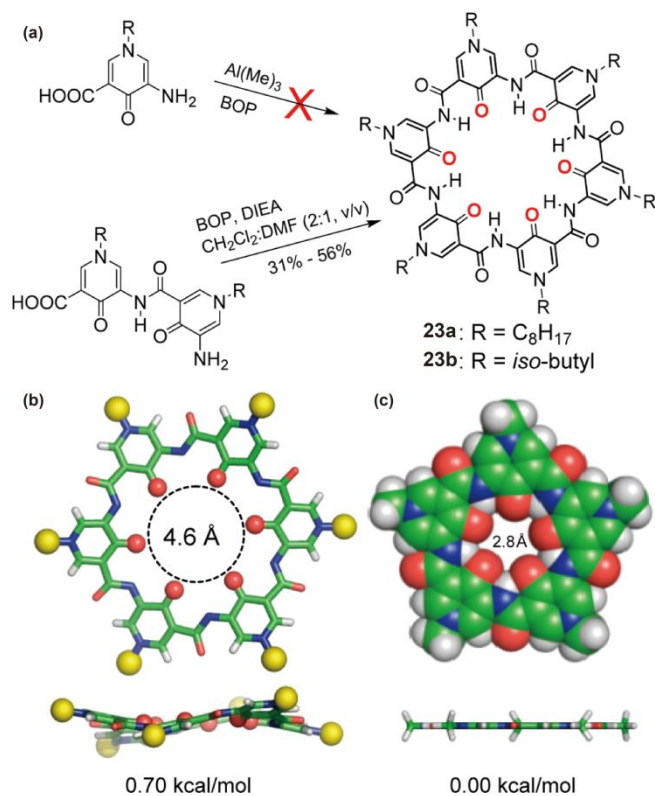


Fig. 20 a) Synthesis of macrocycle **23** using BOP. b) Crystal structure and c) computationally determined structure of **23**. Ref 44

3.2. Non-aggregational Macrocycles with a Fully Constrained Backbone

Macrocycles **18** were developed with the incorporation of peripheral amide groups.⁴⁶ These amide groups were hypothesized to enhance the stacking of the macrocyclic molecules via intermolecular hydrogen bonding. The directionality of multiple hydrogen-bonding interactions may also align the stacked macrocycles, enabling the formation of extended tubular assemblies with enhanced stability.

However, it was found that these macrocycles did not engage in strong aromatic stacking interactions. The ^1H NMR spectra of **18** in a variety of solvents (CDCl_3 , CD_3OD , $\text{DMSO}-d_6$) showed there was insignificant line broadening. With increasing concentration of **18**, the resonances of the backbone protons first underwent significant shifts and then plateaued, remaining as well dispersed signals. This implied that extended aggregation of macrocycle **18** was curbed, i.e., the peripheral amide groups seemed to be discouraging the formation of larger aggregates. The macrocycles were found to form discrete

stacks in solution and in the solid state.⁴⁷ DOSY experiments revealed that these macrocycles assembled into small aggregates at various concentrations, with the tetrameric stack dominating at elevated concentrations. Computational studies revealed that the tetrameric stack was the most stable assembly among lower- or higher-order aggregates.

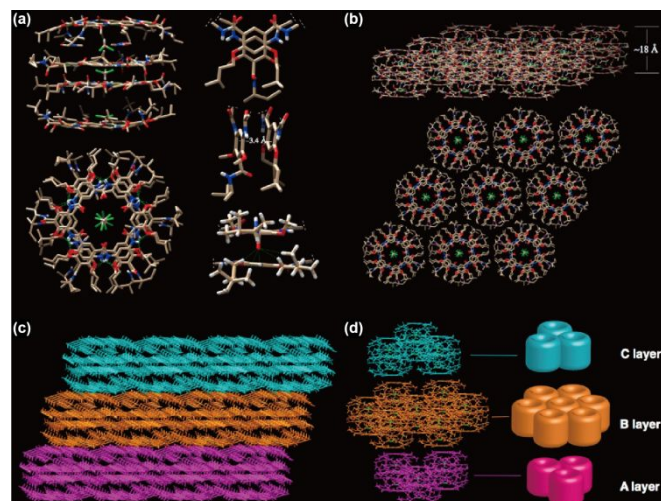


Fig. 21 Crystal structure and further packing of the tetrameric stacks of **11**. (a) Side and top views of the stack. (b) Side and top views of the single layer consisting of hexagonally packed tetrameric stacks. (c) Side view of three stacked layers. (d) Exploded view of the vertical stacking of the 2D. Reprinted with permission from ref. 47. Copyright 2015 American Chemical Society.

The crystal structures of the tetrameric stacks provided details that explained the formation of the discrete complex. In the tetrameric stack, two inner macrocycles stack in a distance of 3.4 Å, with two macrocycles capping the two ends located roughly 7 Å from the inner macrocycles (Fig. 21). The two outer macrocycles were distorted from planarity and existed as shallow bowls. These terminal capping bowls most likely curbed further aggregation due to their protruding amide oxygens which inhibit the further intermolecular associations. Although serendipitously discovered, this discrete self-assembling system provides a rare example of supramolecular oligomerization involving the formation of discrete, rather than extended, stacks of disc-like macrocycles.

Macrocycle **17** was found to bind the guanidinium ion with high affinity and specificity. However, the association constant could not be determined due to the strong aggregation. The second-generation macrocycles **18** enable the quantification of the binding affinity. In CDCl_3 , by extrapolating from solvents containing either $\text{DMSO}-d_6$ or CD_3OD , association constants were found to be in the range of $\sim 10^6 \text{ M}^{-1}$. This discovery prompted further investigations into the modifications of the aromatic oligoamide backbone, since the incorporation of an additional amide group led to macrocycles with significantly changed self-assembling behavior.

3.3. Macrocycles with a Partially Constrained Backbone

Encouraged by the new and unique properties of macrocycles **18**, further modifications based on **18** were made. The alkoxy

side chains flanking each of the peripheral amide groups of macrocycles **18** may have impeded intermolecular stacking interactions. The third-generation macrocycles **19** were designed to alleviate this steric strain, which involved the removal of the alkoxy groups adjacent to the peripheral amide groups.⁴⁸

Interestingly, macrocycles **19**, with their altered backbones, achieved what was previously anticipated with macrocycles **18**. Exceptionally strong aggregation, which outpaced that of the first-generation macrocycles, was observed with macrocycles **19**.⁴⁹ In nonpolar solvents, ¹H NMR revealed little to no signals. These macrocycles also exhibited AIE phenomena which was utilized to study the aggregation. In comparison to **17**, macrocycles **19** exhibited emission intensity that was ten-fold stronger, showing the much greater extent of aggregation. With increasing polar solvent concentrations, downfield chemical shifts were observed for the amide protons of **19**, indicative of attenuated stacking interactions by competitive solvent molecules. At 1 pM, macrocycles **19** underwent a monomer-dimer equilibrium, based on which a lower limit of $4.5 \times 10^{13} \text{ M}^{-1}$ for the dimerization constant was estimated in CHCl₃. Macrocycles **19** were also found to aggregate in stages. Fluorescence spectroscopy revealed an initial fast aggregation followed by slow, gradual aggregation. The fast association resulted in the formation of columnar stacks while the slow aggregations involved the associations of the stacks to form bundles. In the solid state, XRD analysis found typical patterns for columnar stacks of disc-like molecules with up to 60 macrocycles stacking in a continuous fashion. The columnar stacks further pack in a hexagonal lattice.

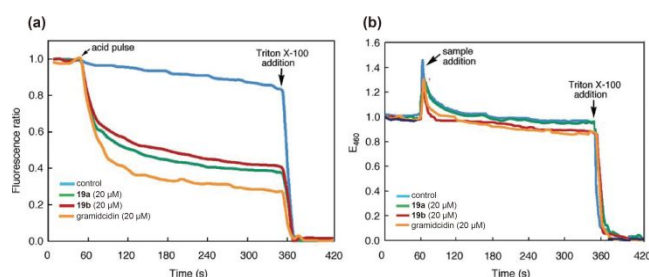


Fig. 22 (a) Time-dependent changes in the (a) ratio of the emission intensities of HPTS (0.1 mM) encapsulated inside 100 nm POPC LUVs in the presence of macrocycle **19** (20 μM) followed by an acid pulse. (b) emission intensity of MQAE (10 mM) encapsulated inside 100 nm POPC LUVs in chloride-free solution incubated with an isotonic buffer containing KCl (100 mM) and followed by aliquots of macrocycles **19** (20 μM) in THF. Reproduced from ref. 49 with permission from the Royal Society of Chemistry.

These studies demonstrated that in solution and solid state, macrocycles **19** can form columnar assemblies with non-deformable, electrostatically negative inner pores. We envisioned that macrocycles **19** could partition into a lipid bilayer to form transmembrane channels like macrocycle **17**. The ability of **19** to transport protons across the membrane was assessed though enclosing the pH-sensitive dye HPTS in a solution of large unilamellar vesicles (LUVs). Upon mixing **19** with the LUVs followed by an extraventricular acid (HCl) pulse, rapid transport of H⁺ across the bilayer was detected (Fig. 22a). Interestingly, this transport was comparable to that of

gramicidin, a well-known channel-forming peptide. We demonstrated through an additional vesicle assay, LUVs enclosing MQAE (a chloride-sensitive fluorescence dye) that these channels do not transport Cl⁻ and thus were selective towards protons in this experiment (Fig. 22b).

3.4. Macrocycles with Hybrid Backbones

Several alternative building blocks and linkages have been investigated over the years leading to hybrid aromatic oligoamide macrocycles. The introduction of alternative building blocks allows for the fine tuning of cavity size and functionality. Incorporation of linkages other than amide bonds such as hydrazide, azo and imine allows for tuning cavity size, photo-switchable conformation, and generation of higher ordered macrocycles through dynamic covalent chemistry, respectively.

Yuan describes a photo-responsive host-guest system constructed from two fully constrained aromatic oligoamide trimers linked via diazenyl bonds.⁵⁰ These diazenyl linkers are photosensitive allowing for conformational control of the macrocycle through cis/trans isomerism (Fig. 23). Under 450 nm the trans isomer is formed and under 365 nm the cis isomer is formed. This resulted in two drastically different macrocyclic conformations which was utilized in the molecular recognition of bipyridinium cations. These macrocycles in the trans conformation were found to bind in a 2:1 stoichiometry however upon irradiation of the complex with 365 nm UV light the guest was released from the complex. Further research using these linkages could afford new host guest systems with superior control.

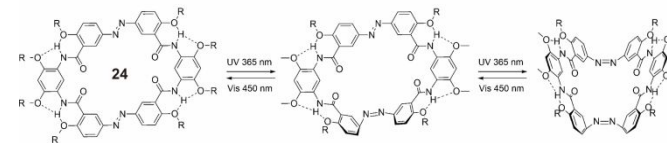
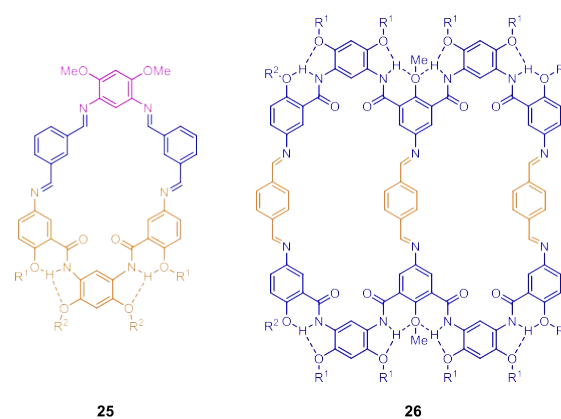


Fig. 23 Photoisomerization of light-responsive azo-macrocycle **24**. Ref 50

Li incorporated dynamic covalent chemistry into the construction of a variety of complex macrocyclic structures. The utilization of the chelate effect through the condensation of backbone rigidified aromatic oligoamides with their corresponding aldehydes lead to highly efficient macrocyclization (Fig. 24).⁵¹ The reversibility of the imine bond allowed for five-component condensations resulting in high ordered macrocyclic cryptands.



25

26

Fig. 24 Aromatic oligoamide macrocycles generated using dynamic covalent chemistry. Ref 51.

Additional hybrid aromatic oligoamide macrocycles were designed in our lab. In our system, the inner cavities of the macrocycles are non-deformable due to the rigid nature of the constrained backbone. With aromatic amide residues, the cavities of these macrocycles are decorated by amide oxygens and cannot be altered. However, the property of the macrocyclic cavity can be tuned through the incorporation of alternative building blocks. Efforts to modify the cavity were realized by substituting one aromatic oligoamide residue with a diethynylbenzene unit, affording a new series of hybrid macrocycles, **20**.⁵² The diethynylbenzene unit introduced into **20** can carry an inward-pointing functional group **X** (**X** = H, CH₃, or NH₂). The aromatic oligoamide segment of **20** would help preserve the strong anisotropic stacking interactions shown by the other macrocycles whereas the new diethynylbenzene unit would enable functionalization of the inner cavity. A secondary amide side chain is attached to the diethynylbenzene unit to reinforce the directionality and stability of the expected tubular assembly of **20** via intermolecular hydrogen bonding.

The aggregation of macrocycles **20** was essentially the same as that of the previous series in both solution and the solid phase, as demonstrated by line-broadening of ¹H NMR signals, enhanced fluorescence emission, and nanofilaments detected by AFM. The aggregation of **20** was enhanced in nonpolar solvents and attenuated in polar solvents.

Macrocycle **20a**, with an inner hydrogen (**X** = H) on the diethynylbenzene unit, enabled much larger proton conductance across the lipid bilayer than those bearing NH₂ or Me groups (Fig. 25a). On the other hand, macrocycle **20d**, with its inner NH₂ group, mediated much more rapid transport of chloride ions and higher Cl⁻/K⁺ permeability ratio, which demonstrated that small modifications to the inner cavity can lead to dramatic change in mass transport properties (Fig 25b).

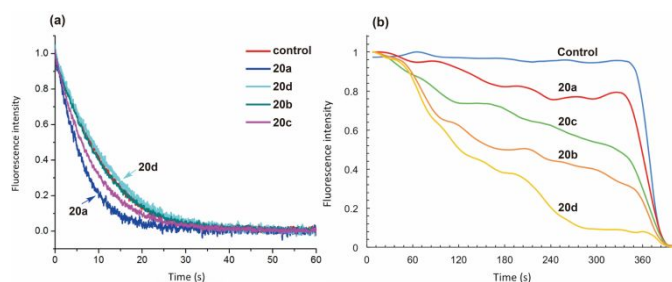


Fig. 25 a) Emission intensity of HPTS (0.1 mM) entrapped in 100 nm POPC LUVs in the presence of macrocycles **20** (10 μM in a pH-7.0 buffer) rapidly mixing with an equal volume of another buffer with 80 mM HCl. b) Normalized emission intensity of MQAE (10 mM) encapsulated inside 100 nm POPC LUVs in chloride-free solution incubated with an isotonic buffer containing KCl (100 mM) and followed by aliquots of macrocycles **20** (10 μM) in THF. Reprinted with permission from ref. 52. Copyright 2016 American Chemical Society.

Typically, water transport channels and pores exhibit hydrophobic inner cavities whereas synthetic systems capable of transporting ions are hydrophilic. The cavity of macrocycles **20**, having both hydrophobic and hydrophilic segments, may allow the transport of water to be controlled. Transmembrane

channel resulted from the stacking macrocycle **20a** was found to facilitate water transport. It was reasoned that the electrostatically negative amide oxygens, which align two thirds of the cavity, can effectively bind metal ions. We found that in the presence of sodium ions, water transport through the channel consisting of stacked **20a** was halted (Fig 26).⁵³ Other alkali metals were found to slow the transport of water but to a much lesser extent, which provide a simple means of fine-tuning.

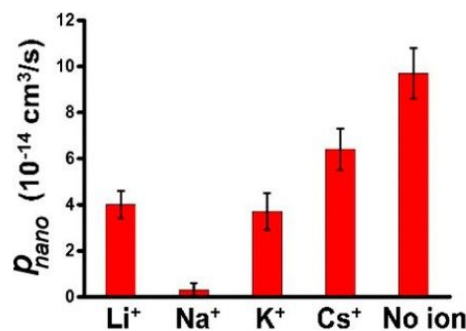


Fig. 26 Measured water permeability P_{nano} through the nanopores formed by **20a**.⁵³

3.5 The Latest-Generation Rigid Macrocycles

The above-discussed aromatic oligoamide macrocycles consist of alternating diacid and diamine building blocks. A new generation of macrocycles was obtained by cyclizing oligoamides with unsymmetrical (*N*-to-*C*) backbones (see Section 2).⁵⁴ This class of aromatic oligoamides fold into well-defined multiturn helices with interesting self-association behavior. Molecular modeling indicated that, among possible macrocycles, the six-residue macrocycles **21** and the seven-residue macrocycles are the least strained. Such macrocycles should readily form by cyclizing the corresponding linear hexa- or hepta-amides which folded into defined crescent conformations that are preorganized for the cyclization. Indeed, macrocycles **21** were obtained in high (~80%) yield by cyclizing the corresponding linear oligoamides without the need to perform the reaction under high dilution condition. Different from the above-discussed macrocycles **17**, **18** and **19**, macrocycle **21** consists of residues that are structurally and electronically identical. As a result, the cavity of macrocycles **21** contains six equidistant carbonyl oxygens. These differences were believed to give rise to potentially new self-assembly and molecular recognition capabilities.

¹H NMR studies indicated that macrocycles **21** also aggregated strongly in nonpolar solvents and were dissociated upon addition of polar solvents. In CDCl₃, no ¹H NMR signals in the aromatic region could be detected. Upon adding up to 20% DMSO-*d*₆, broad featureless peaks emerged. The ¹H NMR signals underwent downfield shift and sharpened up with increasing proportion of DMSO-*d*₆. With roughly 50% DMSO-*d*₆ in the solvent, the ¹H NMR peaks cease to shift, and no further sharpening was observed. Further dilution experiments in this solvent showed that lowering the concentration of the macrocycle resulted in no further change in the ¹H NMR

spectrum, indicating that in this mixed solvent, the macrocycle is molecularly dissolved.

Similar to macrocycles **17** which bind bipyridinium-based guests with high affinity in a 2:1 stoichiometry, macrocycles **21** also bind the same guests in a 2:1 stoichiometry as indicated by mass spectrometry. UV-Vis titration experiments revealed two clearly distinct trend lines, one with a steep slope from 0 to 0.5 equiv of the guest and the other with a zero slope from 0.5 and more equiv of the guest, which further supports the 2:1 binding stoichiometry. Attempts to fit the UV data were unsuccessful presumably due to the steepness of the curve.

The stepwise association constants were determined with ITC experiments which provided the corresponding thermodynamic parameters. Titrating macrocycle **21** into a solution of the bipyridinium guest in DMSO/CHCl₃ (1/1, v/v), two distinct phases were observed in the titration plot. Two transitions were observed, a relatively weak transition near molar ratio 1 and a much stronger transition at molar ratio 2. These curve shapes indicate that for each complexation, the second binding step is stronger than the first binding one, i.e., the host-guest binding exhibits positive cooperativity. Fitting the ITC data using a sequential 2:1 binding model revealed both binding events to be enthalpically and entropically favored. More detailed analysis showed that the first binding event is entropically dominated whereas the second binding event is enthalpically driven. Both binding events are driven by electrostatic interactions between the macrocyclic cavity and the cationic guest. It was speculated that entropic contributions in the first binding event may be due to desolvation of the cavity of the first macrocycle and the bipyridinium guest, whereas the large enthalpic contributions in the second binding event are due to the binding of the second macrocycle to the guest and the strong intermolecular stacking interactions between the two macrocycles in the complex. This also explains the positive cooperativity observed where $K_1 = 10^5$ and $K_2 = 10^6$ based on which an interaction factor α ($\alpha = 4K_2/K_1$) = 42 was obtained.

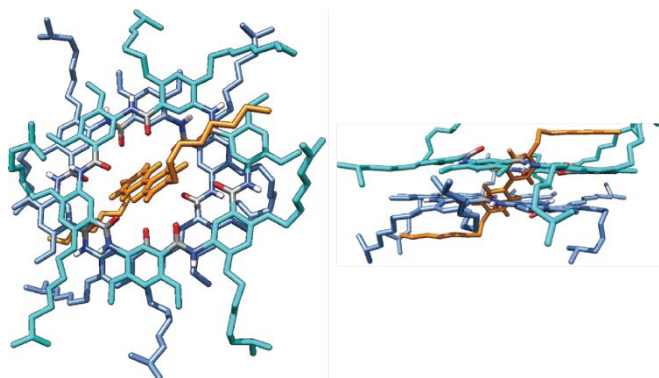


Fig. 27 Top and side views of the crystal structure of pseudo[3]rotaxane formed by **14** and bipyridinium guest. Reproduced from ref. 54 with permission from the Royal Society of Chemistry.

X-ray crystallography of the 2:1 complex between macrocycle **21** and the bipyridinium guest supported the ITC observations as well as shed additional light onto the origins of cooperativity. Within the crystal structure the two macrocycles

are separated by 3.4 – 3.5 Å, indicating strong aromatic stacking interactions (Fig. 27). Also, the octyl tails of the guest are folded back onto the macrocycle backbone serving to anchor the hosts onto the guest scaffold. Additional computational studies found that the final 2:1 complex is more than four times more stable than the intermediate 1:1 complex (Fig. 28).

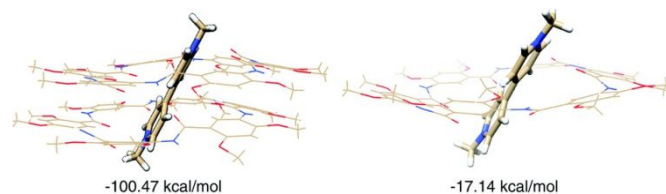


Fig. 28 Energy-minimized structures of the 2:1 complex of **14** (left) and 1 : 1 complex **14** (right) DMSO/CHCl₃ (1/1, v/v). Reproduced from ref. 54 with permission from the Royal Society of Chemistry.

3.6 Macrocycles with Unconstrained Backbones

All previously mentioned aromatic oligoamide macrocycles have some form of backbone constraining intramolecular hydrogen bonding interactions. These rigidifying hydrogen bonding interactions have led to the efficient formation of macrocycles and also preorganized the hosts for interesting self-association and molecular recognition phenomena. In 1995, Kim et al. reported the preparation of macrocycle **27** under high dilution conditions which has the same backbone as **17**, however there is no incorporated intramolecular hydrogen bond.⁵⁵ This macrocycle exhibited very poor solubility however this early example demonstrated that these cyclic oligoamides were capable of recognizing CaCl₂ after organization of the amide N-H groups for convergent interaction with the peripheral chloride atoms within the macrocyclic cavity. Several years later Hamilton further investigated the anion binding potential of unconstrained backbone aromatic oligoamides after the synthesis of a triamide macrocycle, **28**.⁵⁶ Impressively, these macrocycles proved to be efficient receptors for various anions including I⁻, Cl⁻, NO₃⁻, pTsO⁻, HSO₄⁻ and H₂PO₄⁻. The binding stoichiometry was found to be 2:1 (host:guest) where two macrocycles stack to form a sandwich complex. ¹H NMR titration experiments found that titration of the guest into the macrocycle resulted in upfield chemical shifts (aromatic stacking interactions) and further additions of guest causes downfield chemical shifts showing a two-stage binding process. Although no preorganization is implemented into the macrocycle, binding constants up to 10⁴ (M⁻¹) are obtained with H₂PO₄⁻ in pure DMSO-d₆.

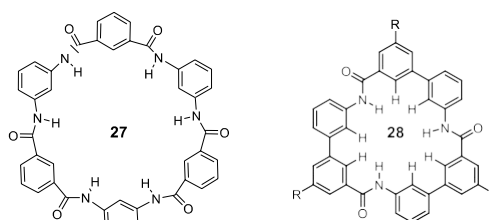


Fig. 29 Unconstrained aromatic oligoamide macrocycles used as anion binders. Refs 55 and 56.

Preorganization has led to the efficient formation of macrocycles however researchers such as Kilbinger have serendipitously obtained impressively high yields from one-pot macrocyclization reactions using an *N*-benzylated phenyl *p*-aminobenzoate monomer in the presence of LiHMDS.⁵⁷ They found that the bulky *N*-benzyl protecting group was essential by sterically hindering intermolecular polymerization and favoring intramolecular cyclization at the linear triamide stage. Later these *N*-benzyl protecting groups could be cleaved to afford a simple para linked continuous backbone trimer aromatic oligoamide. Macrocycle **29** was obtained with an overall yield of 43% over three steps. These deprotected macrocycles exhibited interesting highly ordered H-bonded two-dimensional networks on a calcite surface. Future work using this macrocyclization strategy could afford a whole new series of macrocycles with unconstrained backbones.

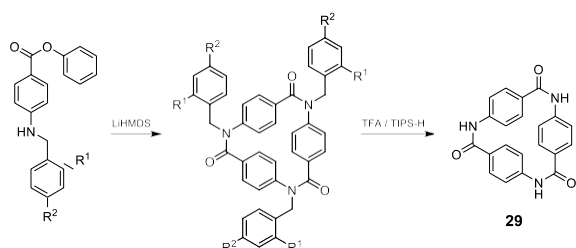


Fig. 30 Synthesis of unconstrained triamide macrocycle **29**. Ref 57.

Recently, Faure has reported a library of novel flexible *N*-substituted aromatic oligoamide macrocycles.⁵⁸ These macrocycles differ by residue number and mode of linkage between residues (*-ortho*, *-meta* or *-para*). The synthesis of the linear precursors was done using solid-phase synthesis and macrocyclization under high dilution conditions afforded macrocycles in yields up to 79%. The lack of intramolecular hydrogen bonding was expected to afford macrocycles with a variety of random conformations, however some of them were found to adopt stable solution state structures. This counterintuitive claim was supported by detailed NMR studies using a combination of COSY, HSQC, HMBC and NOESY. For example, tetramer macrocycle **30** had amides in a stable *cis-trans-cis-trans* configuration in solution which was also apparent in the crystal structure (Fig. 31) The lack of preorganization along the backbone may allow for a diverse array of new architectures. Initial studies found these macrocycles could interact with sodium ions. Further work on these macrocycles could shed light onto the predictability of structure from fundamental sequences.

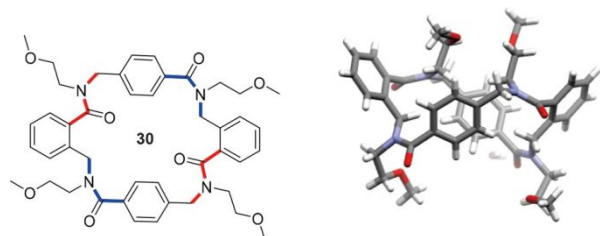


Fig. 31 Left) Conformation of **30** determined by NMR and right) Crystal structure. Ref 58.

4. Anion-Binding Aromatic Oligoamide Foldamers

4.1. Introduction

Over the years lots of attention has been focused on foldamer based cation recognition however the field of anion recognition is underdeveloped. Foldamer based anion recognition developed using the implementation of good hydrogen bond donor moieties such as amide, urea, thiourea, triazole, halogen bonding, indole, and highly polarized C-H bonds for the binding of anions. Foldamer based systems rely on the anion inducing folding of the oligomer to maximize binding potential. Early work by Jeong demonstrated indolcarbazole dimers are capable of folding into compact conformations which are preorganized for binding to various anions, namely sulfate.⁵⁹ Berryman incorporated halogen bonding in the anion induced folding of *m*-arylene-ethynylene oligomers.⁶⁰ These oligomers formed unusual triple helicate supramolecular complexes induced via anion recognition.

4.2. Design and Synthesis

For the aromatic oligoamide foldamers and their corresponding macrocycles we developed have fully constrained backbones with convergently locked amide oxygens and thus possess electronegative cavities or pores. Similarly, foldamers and macrocycles with convergently locked amide NH groups would provide electropositive cavities or pores that would complex anions. However, due to the inherent structural limitations of the amide groups, the creation of aromatic oligoamides with fully constrained backbones carrying inward-pointing amide NH groups still present a daunting, if not impossible, challenge.

Initial aromatic oligoamide-based anion induced foldamers were presented by Li which consist of alternating 1,5-diaminonaphthalene and 1,3-dibenzoic acid monomers (**31** and **32**).⁶¹ These fully unconstrained larger oligomers were constructed with the intention of binding the benzene-1,3,5-tricarboxylate ion (Fig. 32). It was found that these oligomers orientate their amide N-H's in a convergent fashion around the guest molecule resulting in a compact helical conformation in DMSO. The addition of pyrene functional groups at the ends of the oligomers enabled the guest induced folding to be studied using both UV-Vis and fluorescence spectroscopy. With increasing oligomer length the overall association was increased with the longest oligomer (bearing five naphthalene residues) yielding an association constant of $5.5 \times 10^6 \text{ M}^{-1}$ in DMSO.

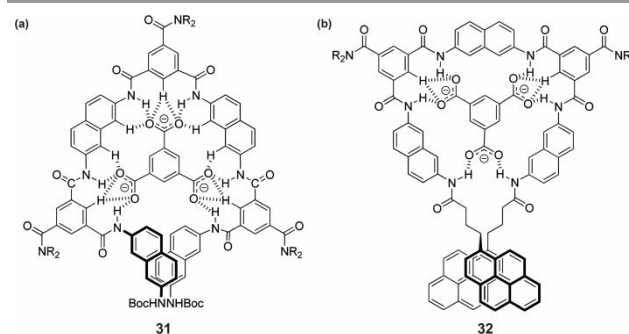


Fig. 32 Anion receptors for binding the benzene-1,3,5-tricarboxylate ion. Ref 61

Our strategy for creating anion-binding aromatic oligoamides involves subjecting a backbone amide carbonyl group to intramolecular hydrogen-bonding interactions with an adjacent NH group provided by an amide sidechain (Fig 33a), which prevents the backbone amide carbonyl oxygen from engaging in additional, undesired hydrogen-bonding interaction and, at the same time, restricts the rotation of the aryl-CO bond.⁶² Oligoamides consisting of such basic units have partially constrained backbones carrying multiple amide NH groups, which, as effective hydrogen-bond donors, should bind anions and other species offering hydrogen acceptors. In the presence of an anion, such an oligoamide, by forming multiple hydrogen bonds with the anion, could convergently orient the amide N-H groups, resulting in a folded crescent or helical conformation (**33•G**).

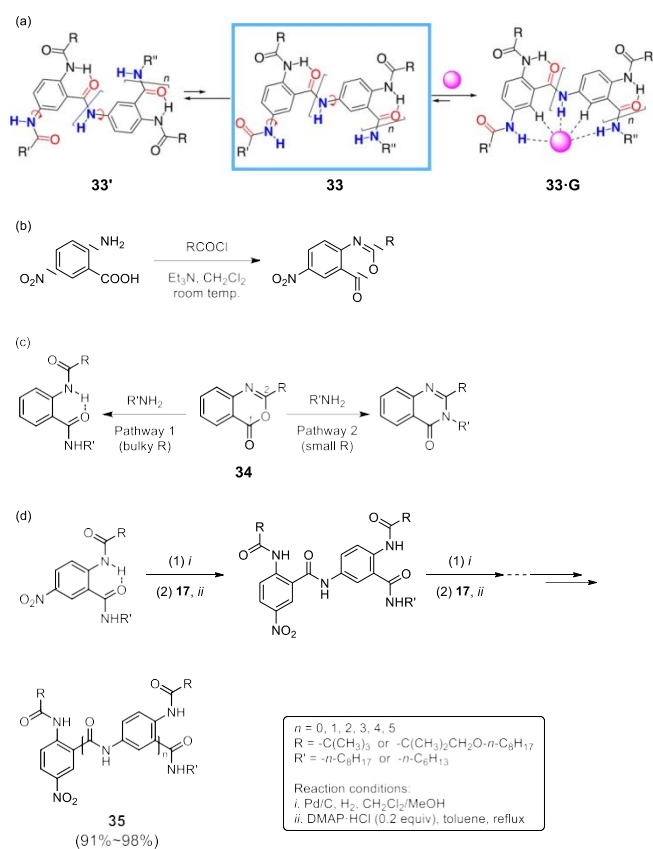


Fig. 33 (a) Instead of adopting multiple conformations as represented by **33'**, oligoamide **33**, upon binding a guest (red sphere) via H-bonding, will be driven to adopt a crescent conformation in which all backbone amide protons and "internal" aromatic protons are convergently arranged. (b) Formation of benzoxazinone. (c) Two outcomes for the ring-opening reaction of benzoxazinone with different size of amine. (d) Synthesis of different length oligoamides **35** by repetitively coupling building blocks derived from 5-aminoanthranilic acid. Reproduced from ref. 62 with permission from the Royal Society of Chemistry.

5-Amino-*N*-acylanthranilic acid serve as the basic building block for these new aromatic oligoamides. Attempts to directly couple the involved building blocks based on established amide-coupling methods all failed, because derivatives of anthranilic acid or *N*-acylanthranilic acid are known to undergo intramolecular cyclization upon treating with acid chloride or coupling reagents to form benzoxazinone derivatives.⁶³ By

probing and optimizing conditions for ring-opening reactions of benzoxazinone **34**, we were able to form the intended amide linkage (Fig 33b-d). This new amide-coupling strategy was then applied to the preparation of oligo(5-amino-*N*-acylanthranilic acids with up to six residues (Fig 33, bottom). The coupling reactions proceeded with high efficiency resulting in >90% coupling yield.

4.3. Anion-Induced Folding

The ability of these new aromatic oligoamides to fold upon binding anions was then studied. Upon treatment of either the tetramer or hexamer with chloride or iodide, downfield shifts were observed for the backbone amide protons, indicative of hydrogen-bonding interactions. Plotting the changes in chemical shifts versus equiv. of the involved anion yielded association constants in the range of 10² for the tetramer (1/9, MeCN-*d*₃/CDCl₃) and 10³ (1/19, DMSO-*d*₆/CDCl₃) for the hexamer. Two-dimensional NMR allowed the conformations of these complexes to be determined. In the absence of anions, the aromatic backbone exists in plethora of conformations. NOEs can be observed between the amide N-H protons and the aromatic protons on both sides of the rings, suggesting a random coil conformation. However, upon addition of an anion most of these NOEs disappear, and clear NOEs are seen between the amide N-H protons and the interior aromatic protons, demonstrating a defined crescent like conformation (Fig. 34). The entropic cost for constraining the oligoamide is compensated by enthalpic gains from the multiple hydrogen-bonding interactions with the anion.

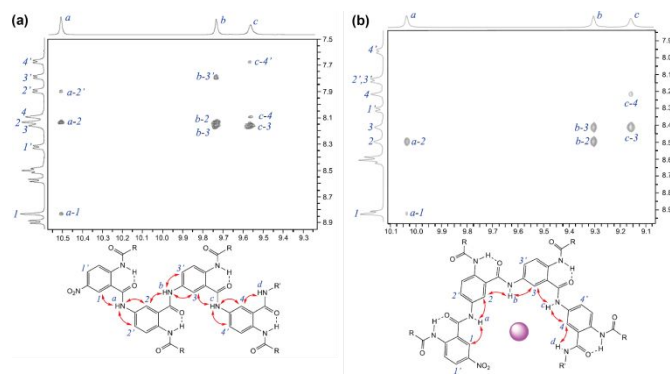


Fig. 34 Partial NOESY spectra of (a) tetramer (5 mM) and (b) tetramer (5 mM) with tetrabutylammonium iodide (5 mM) in CDCl₃ containing 5% DMSO-*d*₆ (500 MHz, 25 °C, mixing time = 0.3 s). The observed NOEs are indicated by double-headed arrows. Reproduced from ref. 47 with permission from the Royal Society of Chemistry.

Conclusions

In this review, we have summarized recent advances in the development of a diverse array of linear and cyclic aromatic oligoamides created by us and others. The incorporation of highly favorable three-center hydrogen bonds along the oligoamide backbones has turned out to be an especially effective strategy for enforcing the folding of such oligomers. In fact, the folded conformations of these aromatic oligoamides persist at different

temperatures and in solvents with low to high polarity or with different hydrogen-bonding capabilities. The reliable folding of these oligoamides has provided molecules with predictable and defined shapes, based on which properties such as tuneable aggregation and molecular recognition capabilities have been generated. Recent progress has realized the synthesis of long oligoamides that fold into multi-turn helices based on which highly electronegative cavities with adjustable depth are being created. The folded conformations of non-cyclic oligoamides promote the efficient formation of cyclic oligoamides based on the intramolecular cyclization of the direct oligoamide precursors, by the coupling of shorter oligoamides, or by the one-pot macrocyclization of the corresponding monomers. Starting from the first-generation macrocycles, up to five generations of rigid macrocycles with inner cavities of different properties have been obtained. These macrocycles have demonstrated unique assembling, recognition, and transporting behavior associated with few other systems. Recently, we have embarked on the challenge of creating aromatic oligoamide foldamers and macrocycles that contain electropositive cavities or pores. Latest results demonstrate that our approach has indeed led to such foldamers and macrocycles for binding various anions. Efforts made by many over the last two decades in evolving aromatic oligoamide foldamers and the corresponding macrocycles have been highly rewarding, with much more remaining to be explored and uncovered. For example, the molecular recognition capabilities of the multi-turn helices obtained recently remain to be explored. The investigation of the new anion-binding foldamers and the corresponding macrocycles has just started. The cavity- and pore-containing foldamers and macrocycles could be further organized in bulk phase to yield the next-generation nanoporous materials.

Conflicts of interest

There are no conflicts of interest to declare.

Acknowledgements

We thank previous and current students, postdoctoral fellows and collaborators who have made this research possible. B.G. has been supported by the National Science Foundation, the National Institutes of Health, the National Aeronautics and Space Administration, the Office of Naval Research, and the Petroleum Research Fund administered by the American Chemical Society.

Notes and references

- 1 K. A. Dill and J. L. MacCallum, *Science*, 2012, **338**, 1042.
- 2 (a) D. H. Appella, L. A. Christianson, I. L. Karle, D. R. Powell and S. H. Gellman, *J. Am. Chem. Soc.*, 1996, **118**, 13071; (b) D. Seebach, M. Overhand, F. N. M. Kühnle, B. Martinoni, L. Oberer, U. Hommel and H. Widmer, *Helv. Chim., Acta.* 1996, **79**, 913.
- 3 (a) S. H. Gellman, *Acc. Chem. Res.*, 1998, **31**, 173; (b) D. Seebach and J. L. Matthews, *Chem. Commun.*, 1997, 2015; (c) B. Gong, *Chem. Eur. J.*, 2001, **7**, 4336; (d) D. J. Hill, M. J. Mio, M. R. B. Prince, T. S. Hughes and J. S. Moore, *Chem. Rev.*, 2001, **101**, 3893; (e) I. Huc, *Eur. J. Org. Chem.*, 2004, 17. (f) E. A. John, C. J. Massena and O. B. Berryman, *Chem. Rev.*, 2020, **120**, 2759.
- 4 (a) W. S. Horne and S. H. Gellman, *Acc. Chem. Res.*, 2008, **41**, 1399; (b) Y. J. Chung, L. A. Christianson, H. E. Stanger, D. R. Powell and S. H. Gellman, *J. Am. Chem. Soc.*, 1998, **120**, 10555; (c) S. Hanessian, X. H. Luo, R. Schaum and S. Michnick, *J. Am. Chem. Soc.*, 1998, **120**, 8569; (d) L. Szabo, B. L. Smith, K. D. McReynolds, A. L. Parrill, E. R. Morris and J. Gervay, *J. Org. Chem.*, 1998, **63**, 1074; (e) D. Seebach, S. Abele, K. Gademann and B. Jaun, *Angew. Chem., Int. Ed.*, 1999, **38**, 1595; (f) J. S. Nowick, D. M. Chung, K. Maitra, S. Maitra, K. D. Stigers and Y. Sun, *J. Am. Chem. Soc.*, 2000, **122**, 7654; (g) C. W. Wu, T. J. Sanborn, K. Huang, R. N. Zuckermann and A. E. Barron, *J. Am. Chem. Soc.*, 2001, **123**, 6778; (h) V. Semetey, D. Rognan, C. Hemmerlin, R. Graff, J. P. Briand, M. Marraud and G. Guichard, *Angew. Chem. Int. Ed.*, 2002, **41**, 1893; (i) G. L. Butterfoss, B. Yoo, J. N. Jaworski, I. Chorny, K. A. Dill, R. Zuckermann, R. Bonneau, K. Kirshenbaum and V. A. Voelz, *Proc. Natl. Acad. Sci. U. S. A.*, 2012, **109**, 14320; (j) A. Patgiri, S. T. Joy and P. S. Arora, *J. Am. Chem. Soc.*, 2012, **134**, 11495; (k) R. V. Nair, S. Kheria, S. Rayavarapu, A. S. Kotmale, B. Jagadeesh, R. G. Gonnade, V. G. Puranik, P. R. Rajamohan and G. J. Sanjayam, *J. Am. Chem. Soc.*, 2013, **135**, 11477; (l) F. G. A. Lister, N. Eccles, S. J. Pike, R. A. Brown, G. F. S. Whitehead, J. Raftery, S. J. Webb and J. Clayden, *Chem. Sci.*, 2018, **9**, 6860.
- 5 (a) R. S. Lokey and B. L. Iverson, *Nature*, 1995, **375**, 303; (b) J. C. Nelson, J. G. Saven, J. S. Moore and P. G. Wolynes, *Science*, 1997, **277**, 1793; (c) T. V. Jones, R. A. Blatchly and G. N. Tew, *Org. Lett.*, 2003, **5**, 3297; (d) J. L. Hou, X. B. Shao, G. J. Chen, Y. X. Zhou, X. K. Jiang and Z. T. Li, *J. Am. Chem. Soc.*, 2004, **126**, 12386; (e) J. J. van Gorp, J. A. J. M. Vekemans and E. W. Meijer, *Chem. Commun.*, 2004, 60; (f) A. M. Zhang, Y. H. Han, K. Yamato, X. C. Zeng and B. Gong, *Org. Lett.*, 2006, **8**, 803; (g) Y. Hua and A. H. Flood, *J. Am. Chem. Soc.*, 2010, **132**, 12838; (h) S. Mathew, L. A. Crandall, C. J. Ziegler and C. S. Hartley, *J. Am. Chem. Soc.*, 2014, **136**, 16666; (i) H. G. Jeon, J. Y. Jung, P. J. Kang, M. G. Choi and K. S. Jeong, *J. Am. Chem. Soc.*, 2016, **138**, 92; (j) J. Shang, N. M. Gallagher, F. S. Bie, Q. L. Li, Y. K. Y. Che and H. Jiang, *J. Org. Chem.*, 2014, **79**, 5134; (k) T. Hu, A. L. Connor, D. P. Miller, X. Wang, Q. Pei, R. Liu, L. He, C. Zheng, E. Zurek, Z. L. Lu and B. Gong, *Org. Lett.*, 2017, **19**, 2666; (l) C. Z. Liu, S. Koppireddi, H. Wang, D. W. Zhang and Z. T. Li, *Angew. Chem., Int. Ed.*, 2019, **58**, 226.
- 6 D. W. Zhang, X. Zhao, J. L. Hou and Z. T. Li, *Chem. Rev.*, 2012, **112**, 5271.
- 7 Y. Hamuro, S. J. Geib and A. D. Hamilton, *J. Am. Chem. Soc.*, 1997, **119**, 10587.
- 8 (a) B. Gong, *Acc. Chem. Res.*, 2008, **41**, 1376; (b) J. Zhu, R. D. Parra, H. Q. Zeng, E. Skrzypczak-Jankun, X. C. Zeng and B. Gong, *J. Am. Chem. Soc.*, 2000, **122**, 4219.
- 9 C. M. Etter, *Acc. Chem. Res.*, 1990, **23**, 120.
- 10 R. Liu, A. L. Connor, F. Y. Al-mkhaizi and B. Gong, *New J. Chem.*, 2015, **39**, 3217.
- 11 K. Yamato, M. Kline and B. Gong, *Chem. Commun.*, 2012, **48**, 12142.
- 12 B. Gong and Z. F. Shao, *Acc. Chem. Res.*, 2013, **46**, 2856.
- 13 (a) Y. Ferrand and I. Huc, *Acc. Chem. Res.*, 2018, **51**, 970; (b) V. Berl, I. Huc, R. G. Khoury, M. J. Krische and J.-M. Lehn, *Nature*, 2000, **407**, 720; (c) H. Jiang, J. M. Léger and I. Huc, *J. Am. Chem. Soc.*, 2003, **125**, 3448; (d) B. Baptiste, C. Douat-Casassus, K. Laxmi-Reddy, F. Godde and I. Huc, *J. Org. Chem.*, 2010, **75**, 7175; (e) X. Hu, S. J. Dawson, Y. Nagaoka, A. Tanatani and I. Huc, *J. Org. Chem.*, 2016, **81**, 1137; (f) N. Chandramouli, Y. Ferrand, G. Lautrette, B. Kauffmann, C. D. Mackereth, M. Laguerre, D. Dubreuil and I. Huc, *Nat. Chem.*, 2015, **7**, 334; (g) J. Shen, R. Ye, A. Romanies, A. Roy, F. Chen, C. Ren, Z. Liu and

- H. Zeng, *J. Am. Chem. Soc.*, 2020, **142**, 10050; (h) G. M. Burslem, H. F. Kyle, P. Prabhakaran, A. L. Breeze, T. A. Edwards, A. S. Nelson, S. L. Warriner and A. J. Wilson, *Org. Biomol. Chem.*, 2016, **14**, 3782; (i) A. F. Kleman, D. L. Dufek, T. L. Fobe, D. R. McCaslin, B. P. Cary, M. R. Shirts and S. H. Gellman, *Org. Lett.*, 2021, **23**, 4855.
- 14 J. Zhu, R. D. Parra, H. Zeng, E. Skrzypczak-Jankun, X. C. Zeng and B. Gong, *J. Am. Chem. Soc.*, 2000, **122**, 4219.
- 15 B. Gong, *Eur. J. Chem.*, 2001, **7**, 4336.
- 16 X. Li, T. Qi, K. Srinivas, S. Massip, V. Maurizot and I. Huc, *Org. Lett.*, 2016, **18**, 1044.
- 17 A. Zhang, J. S. Ferguson, K. Yamato, C. Zheng and B. Gong, *Org. Lett.* 2006, **8**, 5117.
- 18 B. Baptiste, C. Douat-Casassus, K. Laxmi-Reddy, F. Godde and I. Huc, *J. Org. Chem.*, 2010, **75**, 7175–7185.
- 19 X. Hu, S. J. Dawson, Y. Nagaoka, A. Tanatani and I. Huc, *J. Org. Chem.*, 2016, **81**, 1137–1150.
- 20 J. Cao, M. Kline, Z. Chen, B. Luan, M. Lv, W. Zhang, C. Lian, Q. Wang, Q. Huang, X. Wei, J. Deng, J. Zhu and B. Gong, *Chem. Commun.*, 2012, **48**, 11112–11114.
- 21 S. Pal, D. P. T. Nguyen, A. Molliet, M. Alizadeh, A. Crochet, R. D. Ortuso, A. Petri-Fink and A. F. M. Kilbinger, *Nature Chemistry*, 2021, **13**, 705–713.
- 22 J. Shen, R. Ye, Z. Liu and H. Zeng, *Angewandte Chemie International Edition*, 2022, **61**, e202200259.
- 23 Y. Zhong, B. Kauffmann, W. Xu, Z.-L. Lu, Y. Ferrand, I. Huc, X. C. Zeng, R. Liu and B. Gong, *Org. Lett.* 2020, **22**, 6938.
- 24 Y. Ferrand and I. Huc, *Acc. Chem. Res.*, 2018, **51**, 970–977.
- 25 N. Chandramouli, Y. Ferrand, G. Lautrette, B. Kauffmann, C. D. Mackereth, M. Laguerre, D. Dubreuil and I. Huc, *Nature Chemistry*, 2015, **7**, 334–341.
- 26 Y. Zhao, A. L. Connor, T. A. Sobiech and B. Gong, *Org. Lett.*, 2018, **20**, 5486.
- 27 C.-Z. Liu, S. Koppireddi, H. Wang, D.-W. Zhang and Z.-T. Li, *Angewandte Chemie International Edition*, 2019, **58**, 226–230.
- 28 H. Zhao, S. Sheng, Y. Hong and H. Zeng, *J. Am. Chem. Soc.*, 2014, **136**, 14270–14276.
- 29 I. Arrata, C. M. Grison, H. M. Coubrough, P. Prabhakaran, M. A. Little, D. C. Tomlinson, M. E. Webb and A. J. Wilson, *Org. Biomol. Chem.*, 2019, **17**, 3861–3867.
- 30 Z. Hegedus, C. M. Grison, J. A. Miles, S. Rodriguez-Marin, S. L. Warriner, M. E. Webb and A. J. Wilson, *Chem. Sci.*, 2019, **10**, 3956–3962.
- 31 Y. Goto, T. Katoh and H. Suga, *Nature Protocols*, 2011, **6**, 779–790.
- 32 C. Tsiamantas, S. Kwon, C. Douat, I. Huc and H. Suga, *Chem. Commun.*, 2019, **55**, 7366–7369.
- 33 C. Tsiamantas, S. Kwon, J. M. Rogers, C. Douat, I. Huc and H. Suga, *Angewandte Chemie International Edition*, 2020, **59**, 4860–4864.
- 34 L. Yuan, W. Feng, K. Yamato, A. R. Sanford, D. Xu, H. Guo and B. Gong, *J. Am. Chem. Soc.*, 2004, **126**, 11120.
- 35 Y. Yang, W. Feng, J. Hu, S. Zou, R. Gao, K. Yamato, M. Kline, Z. Cai, Y. Gao, Y. Wang, Y. Li, Y. Yang, L. Yuan, X. C. Zeng and B. Gong, *J. Am. Chem. Soc.*, 2011, **133**, 18590.
- 36 X. Li, B. Li, L. Chen, J. Hu, C. Wen, Q. Zheng, L. Wu, H. Zeng, B. Gong and L. Yuan, *Angew. Chem.*, 2015, **54**, 11147.
- 37 A. R. Sanford, L. Yuan, W. Feng, K. Yamato, R. A. Flowers and B. Gong, *Chem. Commun.*, 2005, **37**, 4720.
- 38 X. Li, X. Yuan, P. Deng, L. Chen, Y. Ren, C. Wang, L. Wu, W. Feng, B. Gong and L. Yuan, *Chem. Sci.*, 2017, **8**, 2091.
- 39 A. J. Hesel, A. L. Brown, K. Yamato, W. Feng, L. Yuan, A. J. Clements, S. V. Harding, G. Szabo, Z. Shao and B. Gong, *J. Am. Chem. Soc.*, 2008, **130**, 15784.
- 40 Z. Peng, X. Guo, W. Xu, J. Li, P. Deng, X. Xiao, W. Feng and L. Yuan, *Chem. Commun.*, 2019, **55**, 4869–4872.
- 41 B. Qin, X. Chen, X. Fang, Y. Shu, Y. K. Yip, Y. Yan, S. Pan, W. Q. Ong, C. Ren, H. Su and H. Zeng, *Org. Lett.*, 2008, **10**, 5127–5130.
- 42 B. Qin, W. Q. Ong, R. Ye, Z. Du, X. Chen, Y. Yan, K. Zhang, H. Su and H. Zeng, *Chem. Commun.*, 2011, **47**, 5419–5421.
- 43 C. Ren, V. Maurizot, H. Zhao, J. Shen, F. Zhou, W. Q. Ong, Z. Du, K. Zhang, H. Su and H. Zeng, *J. Am. Chem. Soc.*, 2011, **133**, 13930–13933.
- 44 Z. Du, C. Ren, R. Ye, J. Shen, V. Maurizot, Y. Lu, J. Wang and H. Zeng, *Chem. Commun.*, 2011, **47**, 12488–12490.
- 45 C. Ren, J. Shen and H. Zeng, *Org. Lett.*, 2015, **17**, 5946–5949.
- 46 X. Wu, G. Liang, G. Ji, H.-K. Fun, L. He and B. Gong, *Chem. Commun.*, 2012, **48**, 2228.
- 47 X. Wu, R. Liu, B. Sathyamoorthy, K. Yamato, G. Liang, L. Shen, S. Ma, D. K. Sukumaran, T. Szyperski, W. Fang, L. He, X. Chen and B. Gong, *J. Am. Chem. Soc.*, 2015, **137**, 5879.
- 48 M. Kline, X. Wei and B. Gong, *Org. Lett.*, 2013, **15**, 4762.
- 49 M. A. Kline, X. Wei, I. J. Horner, R. Liu, S. Chen, S. Chen, K. Y. Yung, K. Yamato, Z. Cai, F. V. Bright, X. C. Zeng and B. Gong, *Chem. Sci.*, 2015, **6**, 152.
- 50 Z. Ye, Z. Yang, L. Wang, L. Chen, Y. Cai, P. Deng, W. Feng, X. Li and L. Yuan, *Angewandte Chemie International Edition*, 2019, **58**, 12519–12523.
- 51 J.-B. Lin, X.-N. Xu, X.-K. Jiang and Z.-T. Li, *J. Org. Chem.*, 2008, **73**, 9403–9410.
- 52 X. Wei, G. Zhang, Y. Shen, Y. Zhong, R. Liu, N. Yang, F. Y. Almkhaizim, M. A. Kline, L. He, M. Li, Z.-L. Lu, Z. Shao and B. Gong, *J. Am. Chem. Soc.*, 2016, **138**, 2749.
- 53 Y. Shen, F. Fei, Y. Zhong, C. Fan, J. Sun, J. Hu, B. Gong, D. M. Czajkowsky and Z. Shao, *ACS Cent. Sci.*, 2021, **7**, 2092.
- 54 T. A. Sobiech, Y. Zhong, L. S. Sánchez B., B. Kauffmann, J. K. McGrath, C. Scalzo, D. P. Miller, I. Huc, E. Zurek, Y. Ferrand and B. Gong, *Chem. Commun.*, 2021, **57**, 11645.
- 55 Y. H. Kim, J. Calabrese and C. McEwen, *J. Am. Chem. Soc.*, 1996, **118**, 1545–1546.
- 56 K. Choi and A. D. Hamilton, *J. Am. Chem. Soc.*, 2001, **123**, 2456–2457.
- 57 C. Storz, M. Badoux, C. M. Hauke, T. Šolomek, A. Kühnle, T. Bally and A. F. M. Kilbinger, *J. Am. Chem. Soc.*, 2014, **136**, 12832–12835.
- 58 T. Hjelmgård, L. Nauton, F. De Riccardis, L. Jouffret and S. Faure, *Org. Lett.*, 2018, **20**, 268–271.
- 59 J. Suk and K.-S. Jeong, *J. Am. Chem. Soc.*, 2008, **130**, 11868–11869.
- 60 C. J. Massena, D. A. Decato and O. B. Berryman, *Angewandte Chemie International Edition*, 2018, **57**, 16109–16113.
- 61 Y.-X. Xu, G.-T. Wang, X. Zhao, X.-K. Jiang and Z.-T. Li, *J. Org. Chem.*, 2009, **74**, 7267–7273.
- 62 R. Cao, R. B. Rossdeutcher, X. Wu, B. Gong, *Org. Lett.*, 2020, **22**, 7496.
- 63 G. M. Coppola, *J. Heterocycl. Chem.*, 1999, **36**, 563.